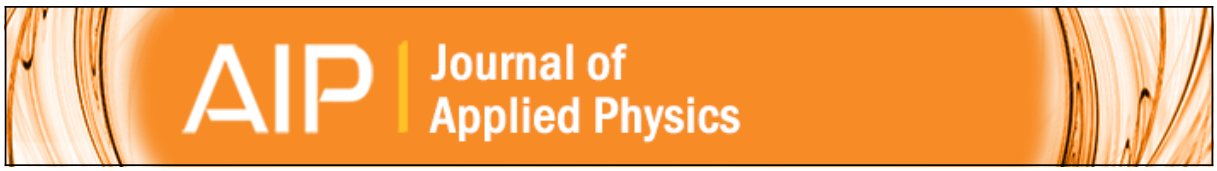

Depth profile study of Ti implanted Si at very high doses

J. Olea, D. Pastor, M. Toledano-Luque, I. Mártil, and G. González-Díaz

Citation: Journal of Applied Physics **110**, 064501 (2011); doi: 10.1063/1.3626466
View online: http://dx.doi.org/10.1063/1.3626466
View Table of Contents: http://scitation.aip.org/content/aip/journal/jap/110/6?ver=pdfcov
Published by the AIP Publishing

[This article is copyrighted as indicated in the article. Reuse of AIP content is subject to the terms at: http://scitation.aip.org/termsconditions. Downloaded to] IP: 147.96.14.16 On: Tue, 11 Feb 2014 19:08:30

Depth profile study of Ti implanted Si at very high doses

J. Olea,[a] D. Pastor, M. Toledano-Luque, I. Mártil, and G. González-Díaz
Dpto. de Física Aplicada III (Electricidad y Electrónica), Facultad de Ciencias Físicas. Universidad Complutense de Madrid, E-28040 Madrid

(Received 27 June 2011; accepted 18 July 2011; published online 16 September 2011)

A detailed study on the resulting impurity profile in Si samples implanted with high doses of Ti and subsequently annealed by pulsed-laser melting (PLM) is reported. Two different effects are shown to rule the impurity profile redistribution during the annealing. During the melting stage, the thickness of the implanted layer increases while the maximum peak concentration decreases (box-shaped effect). On the contrary, during the solidifying stage, the thickness of the layer decreases and the maximum peak concentration increases (snow-plow effect). Both effects are more pronounced as the energy density of the annealing increases. Moreover, as a direct consequence of the snow-plow effect, part of the impurities is expelled from the sample through the surface. © *2011 American Institute of Physics*. [doi:10.1063/1.3626466]

I. INTRODUCTION

In the context of the Third Generation of Solar Cells,[1] the intermediate band (IB) solar cell is one of the most promising concepts to achieve high-efficiency photovoltaic devices at low cost.[2] The basis of this technology is the formation of a semi-filled band inside the traditional forbidden bandgap. This band allows the absorption of low energy photons, which could result in higher efficiency. Many theoretical and experimental attempts have been developed in order to obtain and study IB materials and IB solar cells.[3–11] Recently, the approach of introducing deep level impurities, i.e. chalcogenide elements (such as Te, Se or S) or transition metals (such as Ti), in the Si lattice to form an IB material has been intensely analyzed.[12–18] The aim is to surpass the IB formation limit, i.e., the Mott limit, in order to suppress the Shockley-Read-Hall recombination induced by the presence of deep levels at low concentration,[19] preventing the degradation of the lifetime of carriers. It has been theoretically deduced that this limit could be close to $5.9\text{x}10^{19}$ cm^{-3} for a semi-filled IB (Ref. 20). Moreover, ab-initio calculations predict that interstitial Ti might form a semi-filled IB in Si if the impurity concentration is high enough.[21]

Regarding the experimental procedures to obtain IB materials, ion implantation is the most effective technique to lodge impurities in the semiconductor lattice. The implantation is usually followed by a thermal annealing process to recover the crystalline structure. Due to the fact that deep level impurities usually have a very low solid solubility limit,[22] reaching the Mott limit in a high crystal quality lattice seems to be a difficult task. Although rapid thermal annealing might improve the solubility of impurities,[23] pulsed-laser melting (PLM) annealing has proved to be a more suitable technique to overcome the Mott limit and to obtain supersaturated Si structures with good lattice quality.[12,17] Moreover, PLM has been also used to form IB materials based on the highly mismatched alloys approach.[3,4,24] In the PLM process, a surface layer of the sample is melted and then solidified by liquid-phase epitaxy, producing an intense solute trapping that could overcome the equilibrium solid solubility limit. A single-crystal layer with high lattice quality can be obtained by adjusting the parameters of the annealing process.[17,25,26] The thickness of the melted layer during the PLM depends not only on the parameters of the annealing, but also on the degree of crystallinity of the layer after the implantation process.[27]

With the combination of ion implantation and PLM, single-crystal Si implanted with Ti concentration over the Mott limit have been achieved.[17] Moreover, Ti impurities are mostly located at interstitial positions, and as it has been suggested by theoretical calculations, this is the adequate position to form a metallic IB (Ref. 21). As a result, the formation of an IB has been demonstrated by the characterization of the electronic transport properties[15,16,18] and the optical absorption coefficient at energies below the bandgap.[28] However, being the absorption coefficient extremely high, the very thin layers produced up to date would not absorb most of the incident light. In order to fabricate a highly efficient IB solar cell thicker layers have to be fabricated. The results contained in this paper will help to optimize the fabrication parameters.

In order to verify the suitability of ion implantation followed by a PLM process to obtain an impurity concentration over the Mott limit, and therefore to form an IB, measurement of the thickness of the supersaturated layer and the shape of the impurity profile is required. For this task, time-of-flight secondary ion mass spectroscopy (ToF-SIMS) is a unique tool.[29] Additionally, a correlation between the crystal quality of the resulting layers and the fabrication parameters is extremely important in order to optimize the ion implantation and PLM processes. To achieve this task, transmission electron microscopy (TEM) is used.

II. EXPERIMENTAL

Si samples with (111) orientation and high resistivity ($\sim$200 Ωcm) were implanted with $^{48}\text{Ti}^{+}$ doses in the 10^{15} – 5×10^{16} cm^{-2} range, at energies in the 25 – 30 keV range,

[a]Electronic mail: oleaariza@fis.ucm.es.

 © 2011 American Institute of Physics

[This article is copyrighted as indicated in the article. Reuse of AIP content is subject to the terms at: http://scitation.aip.org/termsconditions. Downloaded to] IP: 147.96.14.16 On: Tue, 11 Feb 2014 19:08:30

using a Varian CF3000 ion implanter refurbished by IBS (France). After implantation, samples were PLM annealed in air with one 20 ns long pulse of a KrF excimer laser (248 nm) with energy densities in the 0.2 – 0.8 J/cm^2 range at J. P. Sercel Associates Inc. (New Hampshire, USA). The KrF laser beam was homogenized, resulting in a 1x1 mm^2 homogenously annealed area per shot. In order to irradiate the entire area of the sample, overlapped annealing steps were performed, with an overlap less than 10 microns long per step.

Ti depth profiles in the Si lattice were obtained by ToF-SIMS measurements carried out with a TOF_SIMS IV equipment manufactured by ION-TOF (Germany), using a 25 keV pulsed Ga^+ ion beam at 45° incidence and O_2 flow. The secondary ions generated were extracted with a 10 keV voltage and their time of flight from the sample to the detector was measured in a reflection mass spectrometer.

Cross sectional TEM images of the samples PLM annealed at 0.8 J/cm^2 were obtained by a JEOL JEM-2000FX microscopy working at 200 keV.

III. RESULTS AND DISCUSSION

Figure 1 shows the Ti depth profiles obtained by ToF-SIMS after the PLM process for different laser energy densities and implantation doses. The Ti concentration surpasses the theoretical Mott limit[20] for all the analyzed conditions. Nevertheless, the thickness of the layer in which this limit is exceeded is strongly dependent on the fabrication parameters. To obtain thicker layers co-implantation processes with increasing energies should be performed. The influence of lattice quality and the formation of secondary phases, which are essential characteristics in the designing of an IB material, have been reported elsewhere.[17] Moreover, from Rutherford backscattering spectroscopy (in random and channeling configuration), it has been pointed out that PLM annealing results in Ti occupying mostly interstitial locations in the Si lattice,[16] as it is required for IB formation in Si (Ref. 21).

The PLM process can be described by two different stages.[26,30] In the first stage, a superficial layer of the sample is melted. The impurities within this layer tend to spread homogeneously in the melted region, as the diffusion coefficients and the solubility limit are orders of magnitude higher than in the solid phase. A box-shaped profile of impurities is therefore obtained. As a consequence of this box-shaped effect, the tail in the impurity profile becomes very sharp and abrupt. This is an interesting result for IB materials, as the impurity concentration below the Mott limit in the tail could deteriorate the IB solar cell performance by increasing the Shockley-Read-Hall recombination and thus decreasing the lifetime of carriers in the device.[19,20] This box-shaped profile can be clearly observed in Fig. 1(d). The Ti concentration drops about three orders of magnitude in just about 50 nm, which is an extremely abrupt profile. Additionally, as the energy density of the PLM annealing increases, the thickness of the melted layer grows, and consequently the height of the box-shaped profile decreases [see Fig. 1(d)].[12,25,31]

In the second stage, the melted layer begins to solidify, and the melted front moves forward from the non-melted edge of the substrate to the surface, pushing the impurities in the process. In this stage the thickness of the impurity profile tends to decrease because of the pushing effect. Regarding the impurity concentration, a snow-plow effect takes place, causing an increase of the height of the profile near the surface due to the accumulation of impurities [see Fig. 1(a)].

These two stages have somewhat opposing effects on the thickness of the supersaturated layer and on the

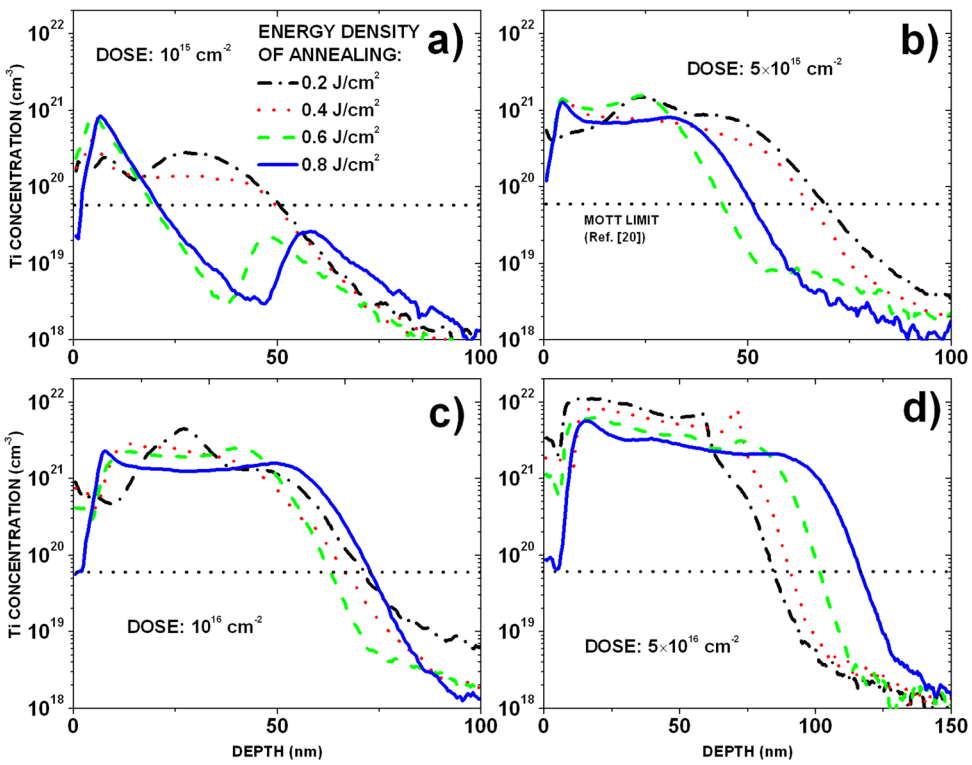

FIG. 1. (Color online) ToF-SIMS Ti depth profiles of Si samples implanted with Ti doses in the $10^{15} - 5\times10^{16}$ cm^{-2} range, and subsequently PLM annealed with one KrF pulse with energy density in the 0.2 – 0.8 J/cm^2 range. The theoretical Mott limit from Ref. 20 is also shown. (a) Dose: 10^{15} cm^{-2}, (b) dose: 5×10^{15} cm^{-2}, (c) dose: 10^{16} cm^{-2} and (d) dose: 5×10^{16} cm^{-2}.

[This article is copyrighted as indicated in the article. Reuse of AIP content is subject to the terms at: http://scitation.aip.org/termsconditions. Downloaded to] IP: 147.96.14.16 On: Tue, 11 Feb 2014 19:08:30

maximum of the impurity profile. The resulting shape of the impurity profile depends mostly on the parameters of the annealing, such as wavelength, energy density and pulse duration,[26] and on the degree of crystallinity after the implantation process.[27] This degree of crystallinity is determined mainly by the element implanted, and by the energy and dose of the implantation.

The maximum Ti concentration for all the samples is obtained directly from the profiles in Fig. 1 and it is plotted in Fig. 2 as a function of the implantation dose for all the energy densities used in the annealing processes. As expected, the maximum of the profiles increases as the implanted dose is raised. However, a not so obvious trend related to the competing effects during annealing is also observed. For low implanted doses the peak is higher for higher energy densities, while for high doses the peak is higher for low energy densities. It seems that the box-shaped effect is stronger at high doses while the snow-plow effect dominates at low doses. The crossover between both trends is found for the dose of 5×10^{15} cm^{-2}. For this dose all the profiles have roughly the same maximum concentration.

The depth of the melted layer can be determined from direct observation of the profiles for some process conditions. For example, it is reasonably clear that the melted depth of the sample implanted with a dose of 10^{15} cm^{-2} and annealed with an energy density of 0.8 J/cm^2 is at the valley at 45 nm [see Fig. 1(a)]. This valley indicates the beginning of the solidifying front, and the layer beyond this valley would have been only heated but not melted. However, this direct observation of the melted depth is not always possible. On the other hand, the thickness of the layer in which the Mott limit has been surpassed can be easily extracted from the profiles shown in Fig. 1. Since the PLM annealing produces a very abrupt impurity profile, this thickness should be very close to the thickness of the melted layer for samples where most of the implanted layer has been melted.

The thickness of the layer in which the Mott limit has been exceeded is shown in Fig. 3 as a function of the energy density of the annealing for all the implanted doses. For low doses the thickness tends to decrease as the energy density of the annealing increases. This is caused by the snow-plow effect. On the contrary, for the highest dose, the thickness increases when the energy density of the annealing rises. This can be explained by the box-shaped effect. In this case the crossover is at the dose of 10^{16} cm^{-2}. For this dose the thickness of the layer is almost constant regardless of the energy density of the annealing. In conclusion, the study on the melted layer thickness also shows the behavior of the different effects of the two stages taking place during the annealing.

Apart from the parameters of the annealing, the most likely cause of the variation of the peak concentration and the thickness of the melted layer, regarding the box-shaped effect and the snow-plow effect, is the degree of crystalline quality in the layer. This degree can be directly related to the dose of implantation, for a given implanted element implanted and energy of implantation. As the dose is increased, the damage to the lattice turns out to be higher and deeper, and thus the melted region is thicker[27] for a given PLM process. In this case, the box-shaped effect dominates, causing a decrease of the impurity profile peak [see Fig. 1(d)]. On the other hand, for low doses, the minimum required energy density for melting a certain thickness would be higher. Therefore, the melted layer would be thinner, and the decrease of the peak related to the box-shaped effect would be less significant. The snow-plow effect dominates, causing the peak to rise as shown in Fig. 1(a).

The PLM process has also an explosive behavior[32] because the two stages take place in a very short period of time.[33] As a result, the snow-plow effect tends to expel a certain quantity of the implanted impurities out of the sample through the surface. The expelled Ti after the PLM annealing can be easily calculated by integrating the area below the ToF-SIMS profile and relating the result to the implanted dose. The remaining Ti concentration percentage after annealing is plotted in Fig. 4 as a function of the PLM energy

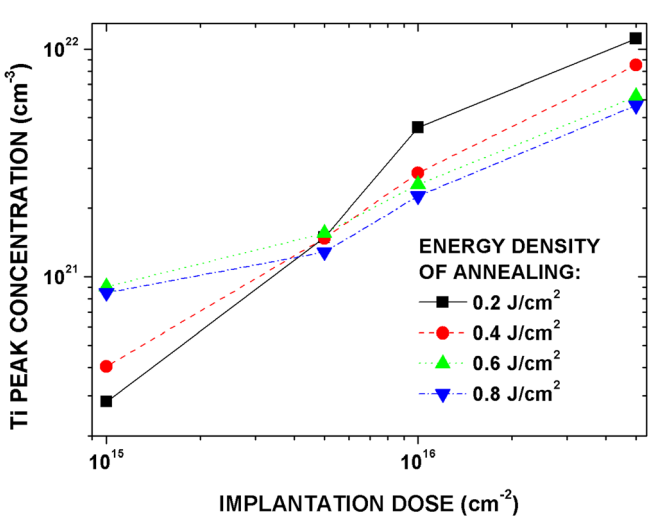

FIG. 2. (Color online) Maximum peak concentration of Ti profiles depicted in Fig. 1 as a function of the implantation dose for all the laser energy densities used in the PLM annealing.

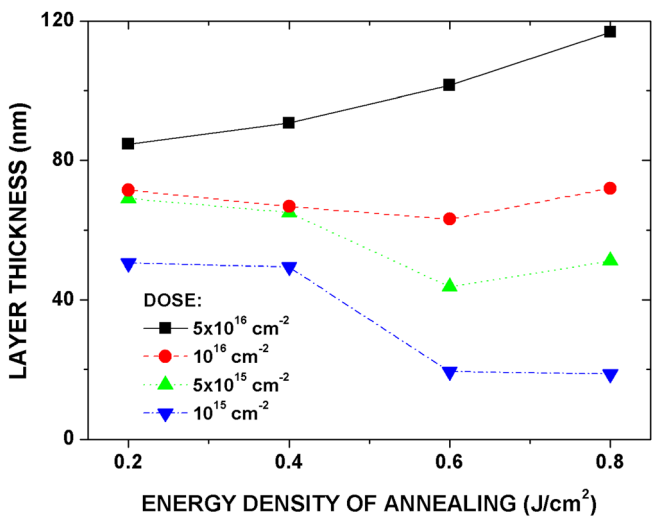

FIG. 3. (Color online) Thickness of the layer in which the Mott limit is exceeded, obtained from Ti profiles depicted in Fig. 1 as a function of the energy density of the PLM annealing for all the implanted doses.

[This article is copyrighted as indicated in the article. Reuse of AIP content is subject to the terms at: http://scitation.aip.org/termsconditions. Downloaded to] IP: 147.96.14.16 On: Tue, 11 Feb 2014 19:08:30

density for all the profiles shown in Fig. 1. For the samples PLM annealed with an energy density of 0.2 J/cm^2 the Ti loss is negligible, so the remaining Ti concentration for these samples has been used as a reference. It has been reported that this energy density is close to the minimum required energy density to melt the surface of an amorphous layer.[27] If the melting does not actually take place, the snow-plow effect would not appear. Intuitively, the remaining Ti decreases as the energy density of the annealing increases, since the duration of the melting is longer.[33] For 0.8 J/cm^2 the remaining Ti after the annealing is in the 52.7 – 81.8% range, depending on the implanted dose. However, even though the Ti loss is high, the remaining concentration is still over the Mott limit. Finally, from the trends presented in Fig. 4, it is concluded that the highest remaining Ti concentration percentage is obtained for an implantation dose of 10^{16} cm^{-2}, for all the analyzed energy densities. As previously discussed concerning the results shown in Fig. 3, for this dose the box-shaped and the snow plow effects are almost compensated, producing a constant thickness. In this case, this equilibrium seems to generate the lowest Ti loss.

The crystalline quality of the implanted layers after the PLM process can be correlated to the depth profile of the Ti impurities by comparing the TEM images and the ToF-SIMS profiles of the samples. This is shown in Fig. 5 for all the implantation doses used for the samples PLM annealed at 0.8 J/cm^2. For each sample the TEM image shows the implanted and PLM annealed layer on top of the substrate, and the ToF-SIMS figure, showing Ti depth concentration, is plotted in the same scale. The theoretical IB formation limit ($\sim 5.9\times10^{19}$ cm^{-3}) (Ref. 20) is also shown. The samples implanted with the highest doses have a poor crystalline quality and a high defect density. Moreover, the sample implanted with the 5x10^{16} cm^{-2} dose exhibits a nanocrystalline character, and the samples implanted with the 10^{16} cm^{-2} and 5x10^{15} cm^{-2} doses have a columnar structure. As the implantation dose is reduced the thickness of the defective layer decreases. An almost perfect recovery of the crystalline structure is achieved for the sample implanted with the lowest dose (10^{15} cm^{-2}).

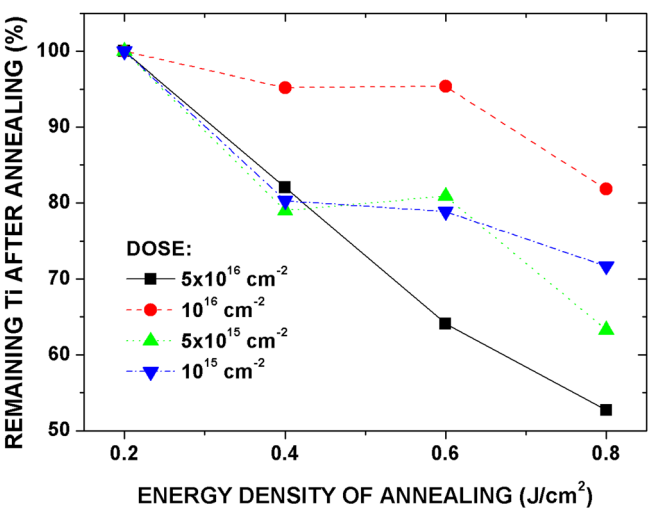

FIG. 4. (Color online) Remaining Ti percentage after PLM annealing as a function of the energy density for all the implanted doses.

The most probable reason for the formation of these defective layers is the extremely high density of Ti impurities implanted. This high concentration of impurities might introduce an enormous stress in the lattice, and as a result, a good reconstruction is a difficult task. The Ti concentration at the limit of the defective layer is around 2×10^{21} cm^{-3}, 1.5×10^{21} cm^{-3} and 8×10^{20} cm^{-3} for the implantation doses of 5×10^{16} cm^{-2}, 10^{16} cm^{-2} and 5×10^{15} cm^{-2}, respectively. In the case of the sample implanted with 10^{15} cm^{-2}, some defects have been found by high resolution TEM in the area surrounding the peak close to the surface, which has a Ti concentration slightly over 8×10^{20} cm^{-3} (Ref. 17), even though the image presented in Fig. 5 shows no evidence of defects. In conclusion, from the analysis of both TEM and ToF-SIMS data shown in Fig. 5, there seems to be a practical limit for the Ti concentration, close to 10^{21} cm^{-3}, over which the recovery of the crystal lattice by means of PLM annealing might be difficult to achieve. For the KrF excimer laser used, the energy density of 0.8 J/cm^2 is high enough to melt the whole implanted layer.[27] Therefore, this result is not related to an incomplete melting of the implanted layer that could produce a PLM solidifying sub-process starting from a low structural quality seed.[25,26] In the case of the lowest implanted dose (10^{15} cm^{-2}), the implanted layer has a lower amorphous degree. Therefore, the thickness of the melted layer is lower resulting in the observed dip at about 50 nm from the surface in the Ti concentration profile. The absence of this dip in the other samples is a proof of the complete melting of the implanted layer.

The incomplete crystal lattice recovery observed for the samples implanted with the highest doses is probably produced by a breakdown in the interface recrystallization during the layer by layer solidifying process.[34] If the impurity concentration surpasses certain quantity, the interface becomes unstable and the produced layer contains a high density of defects. The main reason for this instability is the accumulation of impurities at the solid-liquid interface during the recrystallization process because of the snow-plow effect. If the breakdown concentration is exceeded, this produces an undercooling of the liquid ahead of the interface and causes the front to be unstable. Moreover, if the interface is not completely planar, impurities tend to segregate to certain locations, and a columnar shape might be produced, being the columns wrapped by a high concentration of impurities. This columnar shape is shown in Figs. 5(b) and 5(c).

However, the concentration of impurities segregating from the interface to the liquid phase might be reduced by increasing the regrowth velocity (reducing the duration of the laser pulse, for example) and thus improving the solute trapping effect. This would stabilize the recrystallization front as there would be less time for the diffusion of the impurities. In this way, good quality layers with higher impurity concentration might be produced. Nevertheless, there still exists a practical limit for the regrowth velocity over which amorphous layers are produced.[35] If the solidifying velocity is increased over this limit, atoms do not have enough time to rearrange, and an ordered lattice is not formed.

[This article is copyrighted as indicated in the article. Reuse of AIP content is subject to the terms at: http://scitation.aip.org/termsconditions. Downloaded to] IP: 147.96.14.16 On: Tue, 11 Feb 2014 19:08:30

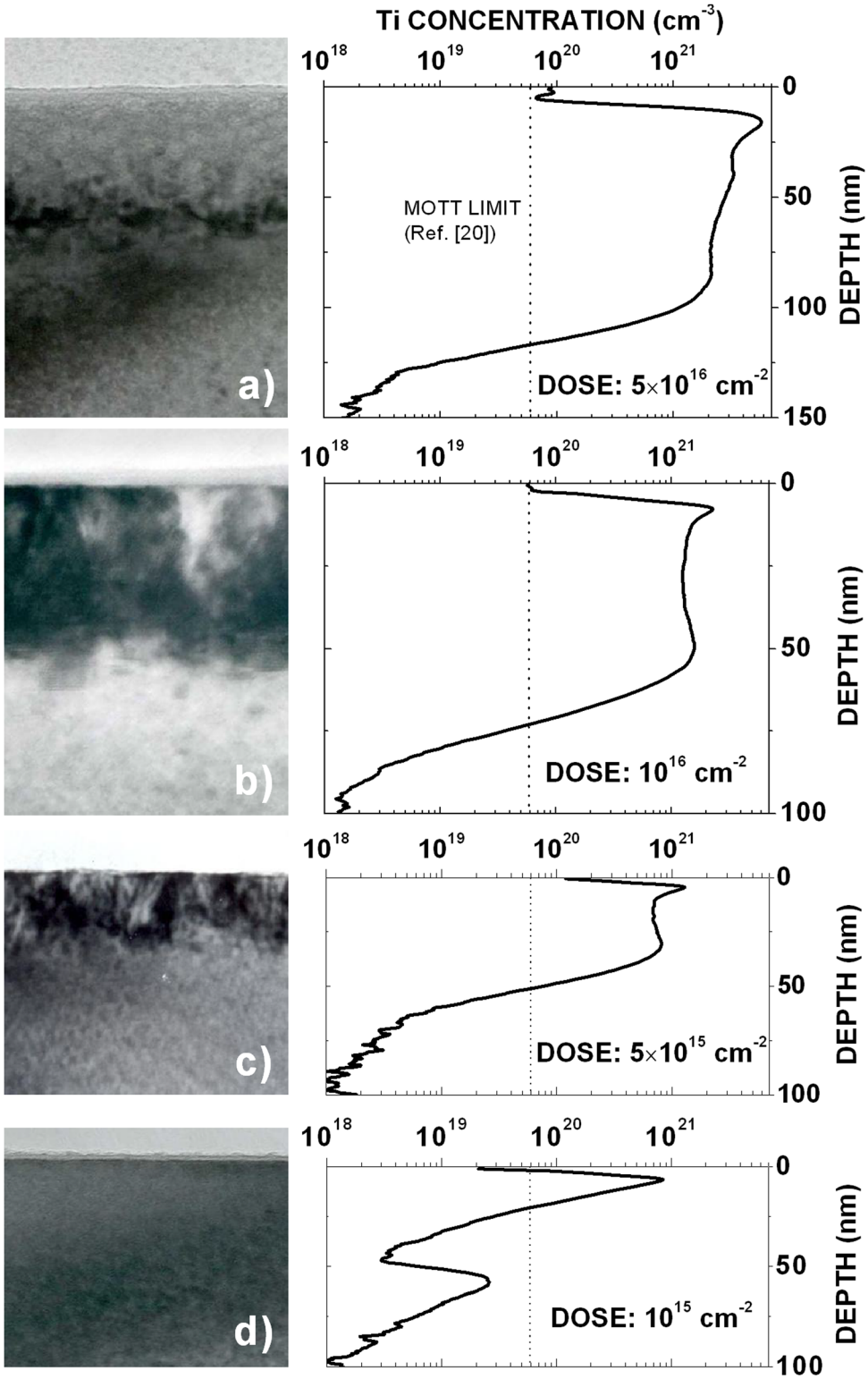

FIG. 5. (Color online) TEM images and ToF-SIMS profiles of the layers PLM annealed at 0.8 J/cm^2 for all the implanted doses. (a) Dose: 5×10^{16} cm^{-2}, (b) dose: 10^{16} cm^{-2}, (c) dose: 5×10^{15} cm^{-2} and (d) dose: 10^{15} cm^{-2}.

IV. CONCLUSIONS

The study of the effects of PLM annealing on the shape of the impurity profile is essential for the research on IB materials based on deep levels introduced by ion implantation. In this paper we have studied these effects with a promising candidate for IB solar cells: Si implanted with high Ti doses. In the melting stage of the annealing, the box-shaped effect produces an abrupt profile. The thickness of the implanted layer tends to increase when the energy density of the annealing is raised, while the maximum peak concentration decreases. In the solidifying stage, a snow-plow effect is observed, and the impurities are pushed through the surface of the sample, decreasing the thickness of the layer and

[This article is copyrighted as indicated in the article. Reuse of AIP content is subject to the terms at: http://scitation.aip.org/termsconditions. Downloaded to] IP: 147.96.14.16 On: Tue, 11 Feb 2014 19:08:30

increasing the maximum peak concentration as the energy density of the annealing goes up. The snow-plow effect is also the origin of the loss of Ti by the surface in the explosive crystallization process. The amorphous degree of the layer after implantation, and ultimately the implantation dose, seems to be the decisive parameter that controls the relative strength of these two competitive effects.

Finally, the formation of defective layers after PLM annealing has been analyzed by means of TEM and ToF-SIMS analysis, yielding a Ti breakdown concentration around 10^{21} cm^{-3} for the annealing conditions used. A Si implanted layer with a Ti concentracion below this limit can be epitaxially recrystalized with a high lattice quality, while a defective solidified layer is obtained when the breakdown concentration is surpassed.

ACKNOWLEDGMENTS

Authors would like to acknowledge the Nanotechnology and Surface Analysis Services of the Universidad de Vigo C.A.C.T.I. for ToF-SIMS measurements, C.A.I. de Microscopía of the Universidad Complutense de Madrid for TEM measurements and C.A.I. de Técnicas Físicas of the Universidad Complutense de Madrid for ion implantation experiments. This work was partially supported by the projects NUMANCIA-II (Grant No. S2009/ENE/1477) funded by the Comunidad de Madrid and GENESIS-FV (Grant No. CSD2006-00004) funded by the Spanish Consolider National Program.

[1]G. F. Brown and J. Wu, Laser Photonics Rev. **3**, 394 (2009).
[2]A. Luque and A. Martí, Phys. Rev. Lett. **78**, 5014 (1997).
[3]K. M. Yu, W. Walukiewicz, J. Wu, W. Shan, M. A. Scarpulla, O. D. Dubon, J. W. Beeman, and P. Becla, Phys. Stat. Solidi B **241**, 660 (2004).
[4]K. M. Yu, W. Walukiewicz, J. W. Ager, III, D. Bour, R. Farshchi, O. D. Dubon, S. X. Li, I. D. Sharp, and E. E. Haller, Appl. Phys. Lett. **88**, 092110 (2006).
[5]P. Palacios, I. Aguilera, K. Sánchez, J. C. Conesa, and P. Wahnón, Phys. Rev. Lett. **101**, 046403 (2008).
[6]W. Wang, A. S. Lin, and J. D. Phillips, Appl. Phys. Lett. **95**, 011103 (2009).
[7]A. Martí, C. Tablero, E. Antolín, A. Luque, R. P. Campion, S. V. Novikov, and C. T. Foxon, Sol. Energy Mater. Sol. Cells **93**, 641 (2009).
[8]T. Tanaka, K. M. Yu, P. R. Stone, J. W. Beeman, O. D. Dubon, L. A. Reichertz, V. M. Kao, M. Nishio and W. Walukiewicz, J. Appl. Phys. **108**, 024502 (2010).
[9]I. Aguilera, P. Palacios, K. Sánchez, and P. Wahnón, Phys. Rev. B **81**, 075206 (2010).
[10]E. Antolín, A. Martí, C. D. Farmer, P. G. Linares, E. Hernández, A. M. Sánchez, T. Ben, S. I. Molina, C. R. Stanley, and A. Luque, J. Appl. Phys. **108**, 064513 (2010).
[11]I. Aguilera, P. Palacios, and P. Wahnón, Sol. Energy Mater. Sol. Cells**94**, 1903 (2010).
[12]T. G. Kim, J. M. Warrender, and M. J. Aziz, Appl. Phys. Lett. **88**, 241902 (2006).
[13]B. P. Bob, A. Kohno, S. Charnvanichaborikarn, J. M. Warrender, I. Umezu, M. Tabbal, J. S. Williams, and M. J. Aziz, J. Appl. Phys. **107**, 123506 (2010).
[14]E. Antolín, A. Martí, J. Olea, D. Pastor, G. González-Díaz, I. Mártil, and A. Luque, Appl. Phys. Lett. **94**, 042115 (2009).
[15]G. González-Díaz, J. Olea, I. Mártil, D. Pastor, A. Martí, E. Antolín, and A. Luque, Sol. Energy Mater. Sol. Cells**93**, 1668 (2009).
[16]J. Olea, G. González-Díaz, D. Pastor, and I. Mártil, J. Phys. D: Appl. Phys.**42**, 085110 (2009).
[17]J. Olea, M. Toledano-Luque, D. Pastor, E. San-Andrés, I. Mártil, and G. González-Díaz, J. Appl. Phys.**107**, 103524 (2010).
[18]J. Olea, G. González-Díaz, D. Pastor, I. Mártil, A. Martí, E. Antolín, and A. Luque, J. Appl. Phys. **109**, 063718 (2011).
[19]A. Martí, L. Cuadra, N. López, and A. Luque, Semiconductors **38**, 946 (2004).
[20]A. Luque, A. Martí, E. Antolín, and C. Tablero, Physica B **382**, 320 (2006).
[21]K. Sánchez, I. Aguilera, P. Palacios, and P. Wahnón, Phys. Rev. B **79**, 165203 (2009).
[22]S. Hocine and D. Mathiot, Appl. Phys. Lett. **53**, 1269 (1988).
[23]D. Mathiot and D. Barbier, J. Appl. Phys. **69**, 3878 (1991).
[24]K. M. Yu, W. Walukiewicz, M. A. Scarpulla, O. D. Dubon, J. Wu, J. Jasinski, Z. Liliental-Weber, J. W. Beeman, M. R. Pillai, and M. J. Aziz, J. Appl. Phys. **94**, 1043 (2003).
[25]R. T. Young, R. F. Wood, J. Narayan, C. W. White, and W. H. Christie, IEEE Trans. Electron. Devices **27**, 807 (1980).
[26]C. W. White, S. R. Wilson, B. R. Appleton, and F. W. Young, Jr., J. Appl. Phys. **51**, 738 (1980).
[27]J. Narayan, C. W. White, M. J. Aziz, B. Stritzker, and A. Walthuis, J. Appl. Phys. **57**, 564 (1985).
[28]J. Olea, A. del Prado, D. Pastor, I. Mártil and G. González-Díaz, J. Appl. Phys. **109**, 113541 (2011).
[29]J. Olea, D. Pastor, I. Mártil and G. González-Díaz, Mater. Res. Soc. Symp. Proc. **1210**, 257 (2010).
[30]B. R. Appleton, C. W. White, B. C. Larson, S. R. Wilson, and J. Narayan, IEEE Trans. Nucl. Sci. **26**, 1686 (1979).
[31]P. Tsouroutas, D. Tsoukalas, I. Zergioti, N. Cherkashin, and A. Claverie, J. Appl. Phys. **105**, 094910 (2009).
[32]C.-C. Kuo, J. Mater. Process. Technol. **209**, 2978 (2009).
[33]G. J. Galvin, M. O. Thompson, J. W. Mayer, R. B. Hammond, N. Paulter, and P. S. Peercy, Phys. Rev. Lett. **48**, 33 (1982).
[34]D. E. Hoglund, M. O. Thompson, and M. J. Aziz, Phys. Rev. B **58**, 189 (1998).
[35]M. O. Thompson, J. W. Mayer, A. G. Cullis, H. C. Weber, N. G. Chew, J. M. Poate and D. C. Jacobson, Phys. Rev. Lett. **50**, 896 (1983).

[This article is copyrighted as indicated in the article. Reuse of AIP content is subject to the terms at: http://scitation.aip.org/termsconditions. Downloaded to] IP: 147.96.14.16 On: Tue, 11 Feb 2014 19:08:30